THE JOURNAL OF PHYSICAL CHEMISTRY C

Article

Cite This: J. Phys. Chem. C 2019, 123, 29922−29931

pubs.acs.org/JPCC

Characterization and Stability of Janus TiXY (X/Y = S, Se, and Te) Monolayers

A. Mogulkoc,[†] Y. Mogulkoc,[‡] S. Jahangirov,[§] and E. Durgun*[,§]

[†]Department of Physics, Faculty of Sciences, Ankara University, Tandogan, 06100 Ankara, Turkey

[‡]Department of Physics Engineering, Faculty of Engineering, Ankara University, Tandogan, 06100 Ankara, Turkey

[§]UNAM - National Nanotechnology Research Center and Institute of Materials Science and Nanotechnology, Bilkent University, 06800 Ankara, Turkey

Supporting Information

ABSTRACT: The realization of Janus MoSSe monolayers has brought two-dimensional (2D), ternary transition metal dichalcogenides (TMDs) into focus. The addition of a third element can lead to superior properties, hence extensive analyses on the characterization of these sophisticated systems are required to reveal their full potential. In this study, we examine the structural, mechanical, electronic, thermal, and optical properties of TiXY (X/Y = S, Se, and Te) monolayers by using first-principles techniques. In addition to the common 1T form, the 2H phase is considered, and the stability of both phases is revealed by phonon spectrum analysis and molecular dynamics simulations. Following the investigation of the mechanical response, electronic structures are examined together with partial density of states analysis. While monolayers of 1T-TiXY are found to be semimetals, monolayers of 2H-TiXY are semiconductors with indirect band gap. The optical spectrum is obtained by calculating the frequency-dependent imaginary dielectric function and is correlated with the electronic structure. The variation of heat capacity with temperature is investigated, and low-/high-temperature response is shown. Finally, possible structural distortions/transformations are also taken into account, and charge density wave transition in 1T-TiSeS due to Peierls instability is demonstrated. Our results not only reveal the stable Janus monolayers of 2H- and 1T-TiXY but also point out these systems as promising candidates for nanoscale applications.

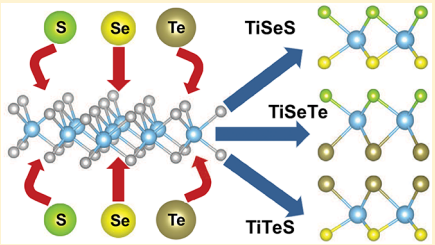

INTRODUCTION

Transition metal dichalcogenides (TMDs) with the chemical formula MX_2 (M = transition metal; X = S, Se, and Te) are a developing class of two-dimensional (2D) materials.[1−5] They possess remarkable properties and exhibit rich chemistry, offering possibilities for both high technological applications and fundamental research.[6] Particularly, their sizable and direct electronic band gaps together with high charge carrier mobility make them suitable for a wide range of devices including but not limited to transistors (FETs),[7] diodes (LEDs),[8] photodetectors,[9] and solar cells.[10] It has been also shown that the inherent properties of TMDs can be further modified by functionalization,[11] phase engineering,[12] strain,[13] applied electric field,[14] and formation of lateral/vertical heterostuctures.[15]

Within the class of TMDs, 2D TiX_2 systems (namely TiS_2,[16,17] $TiSe_2$,[18,19] and $TiTe_2$[20]) which have been synthesized in the 1T phase recently have aroused special interest because of their superior electronic properties and formation of charge density waves (CDWs).[21] Ultrathin nanosheets of TiS_2 have high electrical conductivity (6.76×10^4 S/m),[16] exhibit substantial optical limiting activity,[22] and display enhanced thermoelectric performance with high stability.[23,24] Similar to its bulk counterpart, 2D $TiSe_2$ shows CDW transition at high critical temperature.[25] Additionally, 2D $TiSe_2$ has self-induced superconducting phases that coexist with the CDW order.[26] The monolayer of $TiTe_2$ is a semimetal and also has a CDW phase, while multilayers of it do not exhibit such a transition.[20] These unique properties suggest mono- and multilayers of TiX_2 as ideal platforms for a variety of CDW state related applications including optoelectronic devices and quantum communication.[21]

In addition to binary systems, the growth of the Janus monolayer MoSSe[27,28] by replacing the top S atomic layer with Se atoms has drawn significant attention to 2D ternary TMDs.[28−30] Inclusion of a third element has modified the inherent properties, and an added degree of freedom leads to more appealing functionalities. Following 2D MoSSe, a variety of 2D ternary chalcogenides have been synthesized,[31−36] and many more have been predicted.[37−39] To reveal the potential use of ternary 2D materials in nanoscale applications, it is essential to systematically characterize these systems and investigate the variation of properties with composition and structure.

Motivated with the recent realization of 2D ternary TMDs and novel properties of 2D binary TiX_2 systems, in this study we examine the structural, mechanical, electronic, thermal, and optical properties of TiXY (X/Y = S, Se, and Te) monolayers. In addition to the commonly studied 1T phase, we also consider

Received: July 20, 2019
Revised: November 13, 2019
Published: November 13, 2019

DOI: 10.1021/acs.jpcc.9b06925
J. Phys. Chem. C 2019, 123, 29922−29931

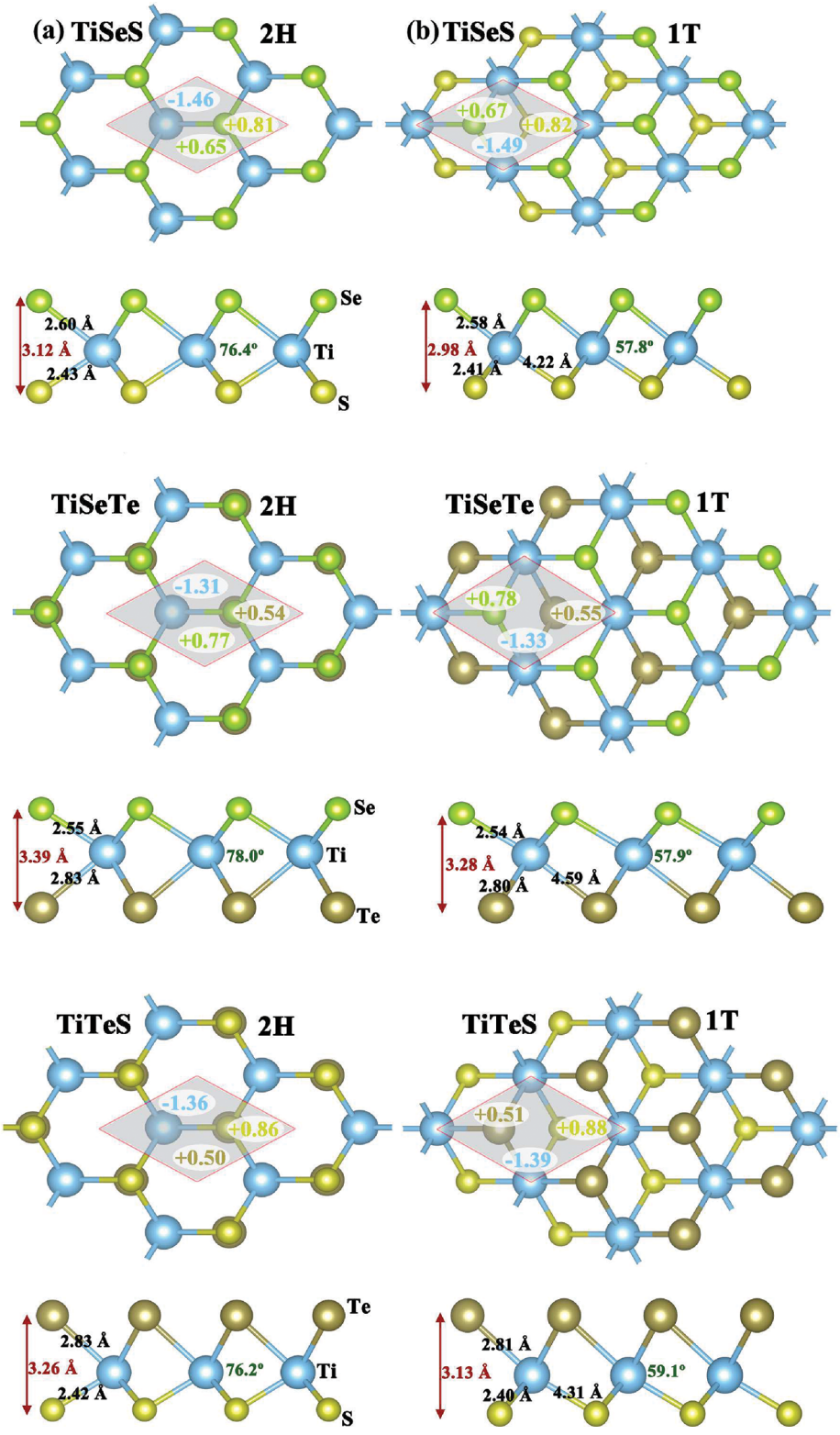

Figure 1. Top and side views of (a) 2H- and (b) 1T-TiXY systems. The shaded area represents the unit cell of the structures. Bader charges are shown on the unit cell in the unit of |e|. Negative (positive) values indicate electron accumulation (donation). Bond lengths (black), bending angles (green), and thickness (red) are shown on the side view.

the 2H polytype and reveal the stability of both phases by phonon spectrum analysis and molecular dynamics (MD) simulations. Following structural optimization, the mechanical response is analyzed, and the Young modulus and Poisson ratio of the considered systems are calculated. Thereafter, electronic structures are examined together with partial density of states analysis. While (undistorted) monolayers of 1T-TiXY are found to be semimetals, monolayers of 2H-TiXY are semiconductors with indirect band gap. The optical spectrum is obtained by calculating the frequency-dependent imaginary dielectric

DOI: 10.1021/acs.jpcc.9b06925
J. Phys. Chem. C 2019, 123, 29922−29931

function and correlated with the electronic structure. The variation of heat capacity within the high/low temperature is also explored. Finally, possible structural distortions/transformations correlated with Peierls instability are also taken into account, and CDW transition in 1T-TiSeS is revealed.

METHODOLOGY

The ground-state electronic structure calculations were performed by using *ab initio* methods based on density functional theory (DFT)[40,41] implemented in Vienna *ab initio* simulation package (VASP).[42] The exchange and correlation effects were described by the generalized gradient approximation (GGA) with the Perdew−Burke−Ernzerhof (PBE) functional.[43] The projector-augmented wave method (PAW)[44,45] was used to interpret the element potentials, and a kinetic energy cutoff of 800 eV was taken for the plane-wave basis set. Atomic positions and lattice constants were optimized by the conjugate gradient method by minimizing the total energy of the system. The convergence criterion for total energy was set to 10^{-8} eV between two sequential steps, and the allowed Hellmann−Feynman force acting on each atom was less than 0.001 eV/Å. Numerical integration over the Brillouin zone (BZ) was performed using the Γ-centered Monkhorst−Pack scheme[46] with a (32 × 32 × 1) k-point mesh. To prevent fictitious interactions between the periodic images, a vacuum spacing of 30 Å was set along the perpendicular direction. In addition to GGA-PBE, the electronic band structures were calculated with a hybrid functional (HSE06),[47,48] which is formed by mixing 25% of the Fock exchange with 75% of the PBE exchange and 100% of the PBE correlation energy. The spin−orbit interactions (SOCs) were also taken into account in the electronic structure calculations. Charge partition of atoms was estimated in the framework of Bader charge analysis.[49,50]

Phonon spectra were obtained by PHONOPY code[51] based on the density functional perturbation theory (DFPT) by considering the 6 × 6 × 1 super cell. The dynamical stability of the systems was further tested by *ab initio* molecular dynamics (MD) calculations using a microcanonical ensemble which scales the atomic velocities at selected temperatures.

The random-phase approximation (RPA)[52] on top of the PBE approach including local field effects was adopted to calculate the optical response. A finer *k*-point sampling (127 × 127 × 1) was used for PBE-RPA calculations, and total number of bands was increased to 96. The linear response of a system due to an external electromagnetic radiation is described by the complex dielectric function $\varepsilon(\omega) = \varepsilon_1(\omega) + i\varepsilon_2(\omega)$. The dispersion of the imaginary part of the complex dielectric function ($\varepsilon_2(\omega)$) was obtained from the momentum matrix elements between the occupied and unoccupied wave functions as follows

$$\varepsilon_2^{(\alpha\beta)} = \frac{4\pi^2 e^2}{\Omega} \lim_{q\to 0} \frac{1}{q^2} \sum_{c,v,\mathbf{k}} 2\omega_{\mathbf{k}} \delta(\epsilon_{c\mathbf{k}} - \epsilon_{v\mathbf{k}} - \omega) \times \langle u_{c+\mathbf{k}+\mathbf{e}_{\alpha q}} | u_{v\mathbf{k}} \rangle \langle u_{c+\mathbf{k}+\mathbf{e}_{\alpha q}} | u_{v\mathbf{k}} \rangle^* \quad (1)$$

where c and v correspond to conduction and valence band states, respectively, and u_{ck} is the cell periodic part of the orbitals at the k-point, **k**.

RESULTS AND DISCUSSIONS

Structural Properties and Stability. Prior to designing ternary systems, we obtain the optimized structures of 2H- and 1T-TiX_2 where X refers to a chalcogen atom (S, Se, or Te). Even 2D TiX_2 is fabricated only in the 1T phase to date, and theoretical analysis also predicted the 2H phase as a stable configuration.[1] Similar to other TMDs, the Ti atom has the six nearest X atoms, and depending on the arrangement of X atoms either a triangular prism (2H) or octahedron (1T) can be formed. The calculated lattice constants (|a|) of 2H−TiS_2, 2H−$TiSe_2$, and 2H−$TiTe_2$ are 3.34, 3.49, and 3.74 Å,[1] and |a| of 1T−TiS_2, 1T−$TiSe_2$, and 1T−$TiTe_2$ are 3.32, 3.43, and 3.64 Å,[2,53,54] respectively. The obtained results are in good agreement with the literature. The binary 2D TiX_2 constitutes the basis of monolayer ternary (Janus) 2H- and 1T-TiXY structures (X/Y = S, Se, and Te). The optimized structures and related structural parameters (bond lengths (d_{Ti-X} and d_{Ti-Y}), thickness (d_{X-Y}), and bond angles (∠X−Ti-Y)) of TiXY monolayers are shown in Figure 1a,b, and the lattice constants are given in Table 1. Similar to binary counterparts, |a| of TiXY also scales with the (average) size of chalcogen atoms. Thus, the smallest and largest |a| is obtained for TiSeS and TiSeTe, respectively. It is observed that |a| of TiXY is in between that of TiX_2 and TiY_2 for both of the phases, and the crystalline symmetry is preserved.

Table 1. Lattice Constant (|a|), Cohesive Energy E_C, Work Function (Φ_w), and Energy Band Gaps (Calculated at the Level of PBE (E_g^{PBE}), PBE-SOC (E_g^{SOC}), and HSE (E_g^{HSE})) of 2H- and 1T-TiXY[a]

phase	structure	|a| (Å)	E_c (eV/cell)	Φ_w (eV)	E_g^{PBE} (eV)	E_g^{SOC} (eV)	E_g^{HSE} (eV)
2H	TiSeS	3.41	10.2	5.96	0.57	0.50	1.34
	TiSeTe	3.61	7.86	5.25	0.16	0.09	0.81
	TiTeS	3.54	9.15	5.22	0.18	0.10	0.77
1T	TiSeS	3.46	10.6	5.44	SM	SM	SM
	TiSeTe	3.64	8.17	4.90	SM	SM	SM
	TiTeS	3.58	9.47	4.89	SM	SM	SM

[a]Semimetallic systems are indicated with SM.

Following the structural optimization, the cohesive energy (E_C) of TiXY monolayers is calculated (per unit cell) using the following expression

$$E_C = E_T(\mathrm{Ti}) + E_T(\mathrm{X}) + E_T(\mathrm{Y}) - E_T(\mathrm{TiXY}) \quad (2)$$

where E_T(Ti), E_T(X), and E_T(Y) correspond to the single atom energies of Ti, X, and Y, respectively, and E_T(TiXY) corresponds to the ground-state energy of the TiXY monolayer. All calculated cohesive energies which are summarized in Table 1 are positive and high (within the range of 8−10 eV), indicating strong binding and stable configurations. E_C decreases down in the chalcogen group for TiX_2, and a similar trend is also noticed for TiXY. Therefore, the highest (lowest) E_C is obtained for TiSeS (TiSeTe). When compared, E_C values of the 1T-phase are higher than those of the 2H-phase (i.e., 1T-phases are more stable than 2H-phases).

As positive E_C is not sufficient to clarify structural stability, phonon spectrum analysis is also performed. The phonon dispersion along the high-symmetry Γ−*K*−*M*−Γ directions is illustrated in Figure 2a,b. The spectrum consists of nine phonon branches where three of them correspond to acoustic modes and the rest are optical modes.[55] The phonon frequencies associated with vibrational normal modes in the BZ are positive for all the considered systems (except 1T-TiSeS), indicating structural stability. Additionally, the Kohn anomaly[56] noticed in TiS_2 is also removed.[2] The phonon branches are shifted to lower frequencies, and the width of the acoustic

DOI: 10.1021/acs.jpcc.9b06925
J. Phys. Chem. C 2019, 123, 29922−29931

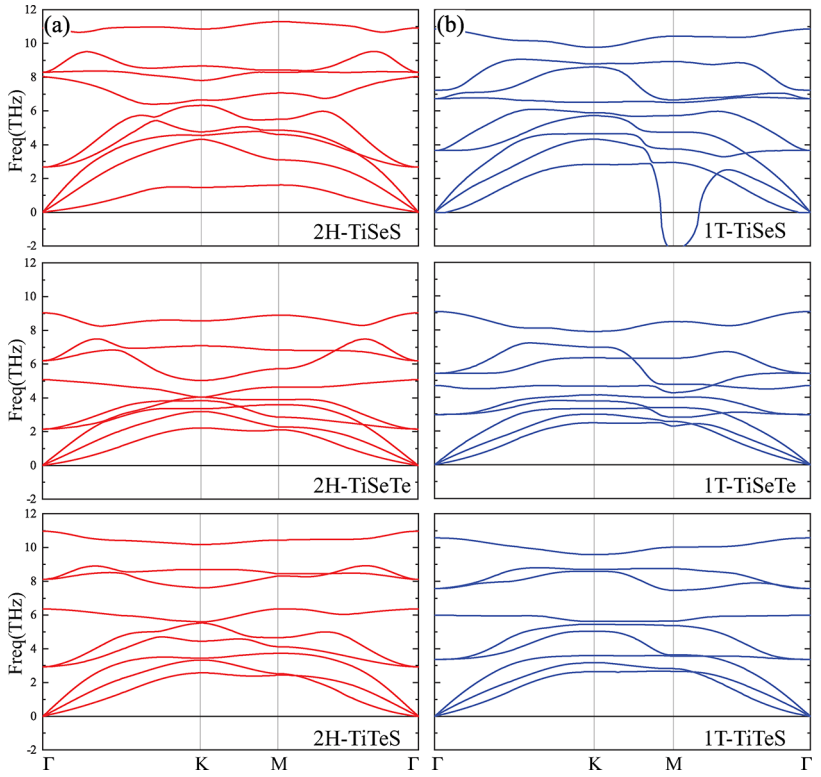

Figure 2. Phonon spectra of (a) 2H- and (b) 1T-TiXY structures.

phonon branches broadens with the increasing mass of chalcogen atoms. TiSeS has the highest TO frequencies ($\Omega(k)$) for both of the phases, and $\Omega(k = 0)$ is nearly 11 THz. For 1T-TiSeS, the ZA phonon branch becomes imaginary around the M point due to Peierls distortion, which results in a CDW transition similar to that observed in 1T-$TiSe_2$.[25,57] Among the considered structures, acoustic branches of TiSeS for both 2H and 1T phases at the vicinity of Γ point are much steeper than the others, indicating a higher thermal conductivity. It is also clear from Figure 2 that there is no gap between acoustic and optical branches for all the structures compatible with their binary counterparts.[54,58−60]

To further test the dynamic stability at high temperatures, *ab initio* MD calculations are performed. The size constraint is removed by taking the 5 × 5 super cell, and then starting from 300 K, the temperature is gradually increased up to 900 K within 3 ps total simulation time. The snapshots of the resulting geometries taken at 900 K are shown in Figure 3a,b. Even at 900 K, atoms only vibrate around their equilibrium positions, which confirmed the dynamical stability of TiXY monolayers at and above ambient temperature.

Mechanical Properties. The mechanical strength of the 2D materials is essential for their use in nanoscale applications. The in-plane stiffness (Y_{2D}) and Poisson's ratio (ν) can be used to characterize the mechanical response of TiXY monolayers, and they are listed in Table 2 together with the relevant elastic constants. First, all calculated elastic constants (C_{ij}) are positive for TiXY, and they satisfy the Born criteria[61] indicating the mechanical stability of these structures. In-plane stiffness can be calculated by using the relation $Y_{2D} = (C_{11}^2 - C_{12}^2)/C_{11}$. It is noticed that Y_{2D} of TiXY monolayers is not the average of its binary counterparts but smaller than those of TiX_2 and TiY_2.[37] Y_{2D} decreases down the group of chalcogen atoms, and thus the smallest value is obtained for TiSeTe. As in-plane stiffness is a

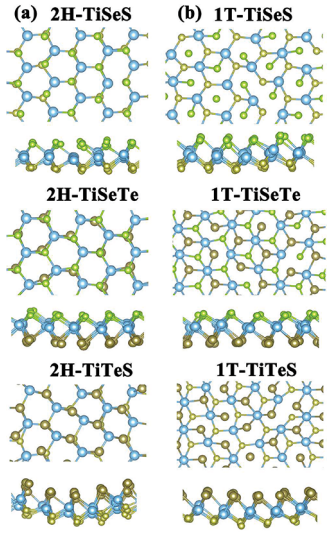

Figure 3. Snapshots of molecular dynamics (MD) simulations of (a) 2H- and (b) 1T-TiXY monolayers taken at T = 900 K.

Table 2. Calculated Elastic Constants (C_{11} and C_{12}), In-Plane Stiffness (Y_{2D}), and Poisson's Ratio (ν) of TiXY Monolayers

phase	structure	C_{11} (N/m)	C_{12} (N/m)	Y_{2D} (N/m)	ν
2H	TiSeS	74.73	26.91	65.04	0.36
	TiSeTe	47.72	24.13	35.52	0.51
	TiTeS	52.30	27.22	38.13	0.52
1T	TiSeS	65.18	16.62	60.94	0.25
	TiSeTe	47.63	15.58	42.53	0.33
	TiTeS	53.27	17.68	47.40	0.33

DOI: 10.1021/acs.jpcc.9b06925
J. Phys. Chem. C 2019, 123, 29922−29931

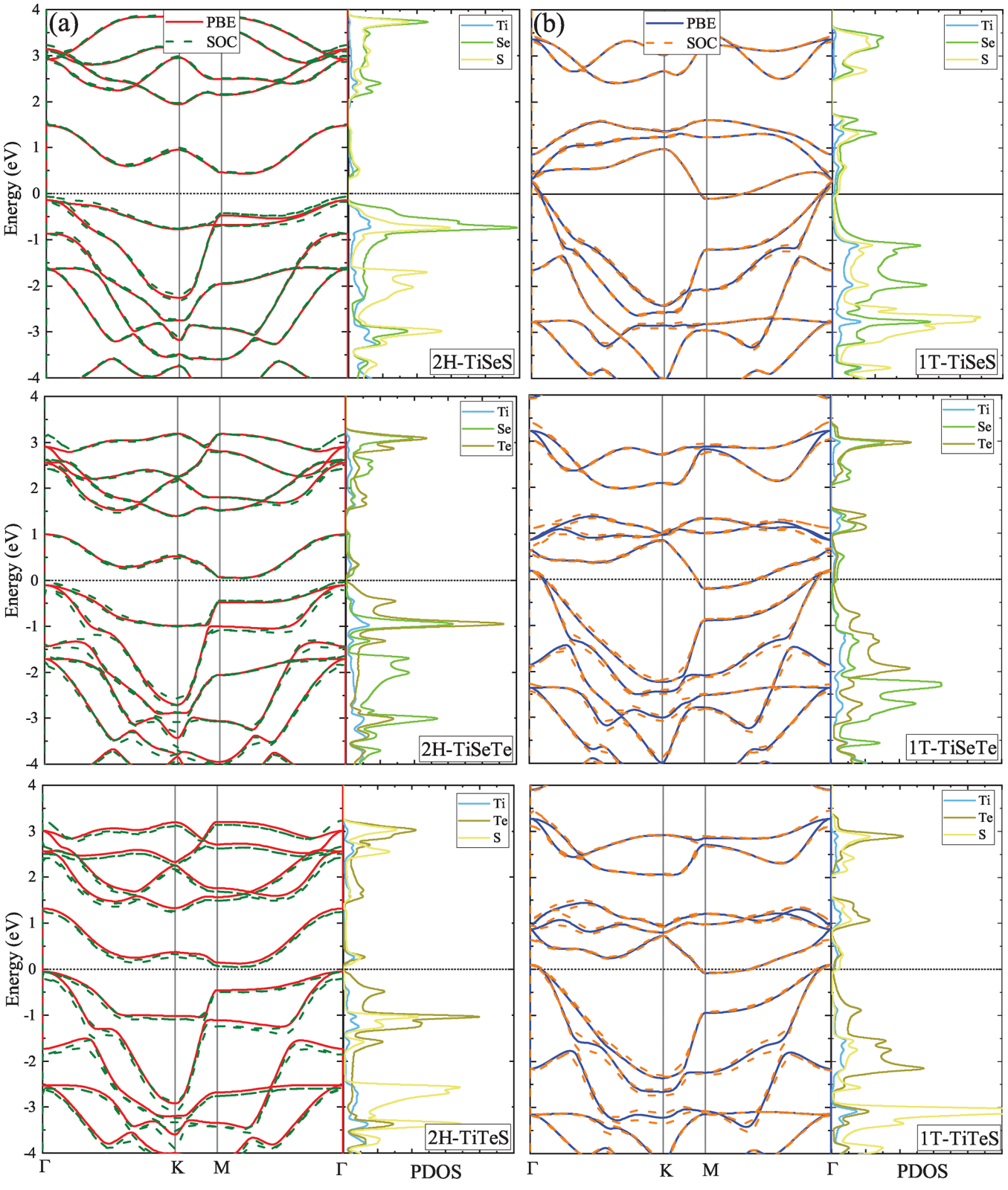

Figure 4. Band diagram and partial density of states (PDOS) of (a) 2H- and (b) 1T-TiXY structures. The effect of spin−orbit coupling (SOC) is shown by dashed lines. Fermi level is set to zero.

measure of rigidity, this decrease indicates softening of the crystal. When compared with other ternary TMDs, Y_{2D} of TiXY is smaller (larger) than those of MoXY and WXY (VXY and CrXY).[37]

In a similar manner, Poisson's ratio ($\nu = \frac{C_{12}}{C_{11}}$) which is the ratio of transverse contraction strain to longitudinal extension strain is calculated. Different from Y_{2D}, ν increases with the increasing atomic number of chalcogen atoms. Additionally, based on Christensen's ductility criterion,[62] while monolayers of

DOI: 10.1021/acs.jpcc.9b06925
J. Phys. Chem. C 2019, 123, 29922−29931

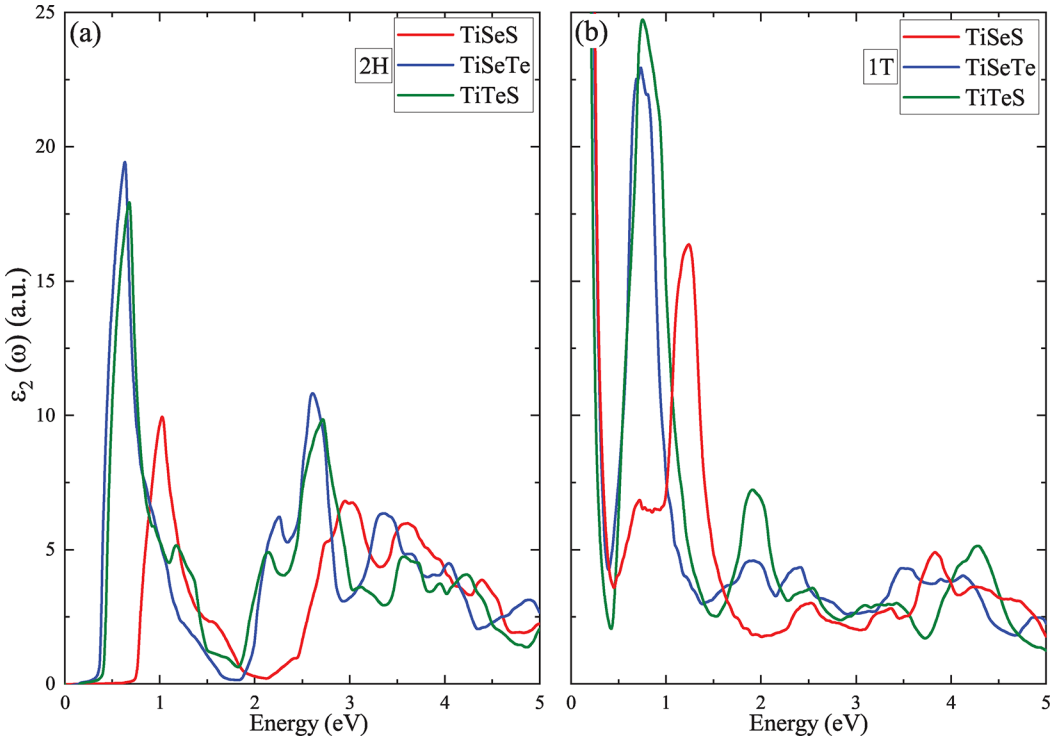

Figure 5. Frequency-dependent imaginary dielectric function ($\varepsilon_2(\omega)$) of (a) 2H- and (b)1T-TiXY monolayers.

1T-TiXY are brittle ($\nu < 1/3$), monolayers of 2H-TiXY are considered to be ductile ($\nu > 1/3$).

Electronic Properties. The calculated electronic band structures for 2H and 1T phases are shown in Figure 4a,b. Similar to their binary counterparts,[2] monolayers of undistorted 1T-TiXY are semimetallic with negative band gap between the two bands crossing the Fermi level (E_F) around the Γ (pockets of electrons) and M point (pockets of holes). Indirect negative band gaps of TiSeS, TiSeTe, and TiTeS at the level of GGA-PBE (+SOC) are calculated as 0.371 eV (0.372 eV), 0.394 eV (0.424 eV), and 0.176 (0.187 eV), respectively. When compared, these values are within the same range but smaller than those reported for binary TiX_2.[53,57] Significantly smaller negative band gaps are calculated with hybrid functionals, but a similar profile is obtained (Figure S1, Supporting Information).

On the other hand, all 2H-TiXY phases are semiconductor as illustrated in Figure 4a. However, the literature on 2H-TiX_2 is scarce,[2] and the monolayer of 2H-$TiTe_2$ is reported as a metal. Accordingly, it can be postulated that broken symmetry due to the addition of a third element turns metallic 2H-TiX_2 into indirect band gap semiconductor 2H-TiXY. The band gap (E_g) decreases down the group of chalcogen atoms, leading to the highest value for 2H-TiSeS (0.57 eV) and the smallest value for 2H-TiTeSe (0.16 eV). The variation of E_g is correlated with the amount of charge donated to Ti from chalcogenides as shown in Figure 1a. The inclusion of spin−orbit coupling (SOC) decreases E_g around 7−8 meV (Table 1). As expected, larger E_g is obtained when calculations are repeated by HSE functional; however, similar trends are observed. E_g^{HSE} values are summarized in Table 1, and the corresponding band structures are provided in Figure S1 (Supporting Information). To get better insight about the electronic properties of the structures, the partial density of states (PDOS) are also examined (Figure 4). When the states in the vicinity of E_F are considered, chalcogen atoms mainly (but unevenly) contribute to the valence band maximum (VBM) and conduction band minimum (CBM) states. As bands below E_F are less dispersive for 2H-TiXY than those of 1T-TiXY, sharper peaks in PDOS are obtained for 2H-TiXY.

From Table 1, it follows that the investigated 2H- and 1T-TiXY monolayers have work functions (Φ_w) between 4.89 and 5.96 eV. When compared, semiconductor H-phases have higher Φ_w values than semimetallic T-phases, and Φ_w decreases down the chalcogen group following a trend similar to E_g. Calculated work functions are comparable with those of various TMDs.[63] The high Φ_w leads to better carrier injection efficiency from metal to TiXY in electronic devices and can lower the contact resistance at the interface.[64]

Optical Properties. The in-plane optical responses of 2H- and 1T-TiXY monolayers are analyzed by calculating the imaginary part of dielectric function ($\epsilon_2(\omega)$) which is presented in Figure 5a,b. The absorption onsets of semiconducting 2H-TiXY are correlated with their electronic band gaps. Thus, the onset of absorption redshifts down the group of chalcogen atoms. Considering the HSE-corrected optical spectrum (Figure S2, Supporting Information), 2H-TiSeS has a significant absorption in the visible region, while absorption of 2H-TiSeTe and 2H-TiTeS remains in the infrared region. Additionally, all systems have secondary remarkable absorption peaks at the near-UV region.

For metallic 1T-TiXY, a Drude peak is obtained due to the free carrier intraband transitions in the low-frequency regime. The main absorption peaks of 1T-TiSeS, 1T-TiTeS, and 1T-TiTeSe are located at 1.02, 0.75, and 0.68 eV, respectively, all remaining in the infrared regime.

Thermal Properties. Associated with the analysis of the phonon modes, we also calculate the heat capacity (C_v) of 2H- and 1T-TiXY monolayers excluding the electronic contributions (which are negligible at all practical temperatures). C_v determines not only the thermal energy stored within the

DOI: 10.1021/acs.jpcc.9b06925
J. Phys. Chem. C 2019, 123, 29922−29931

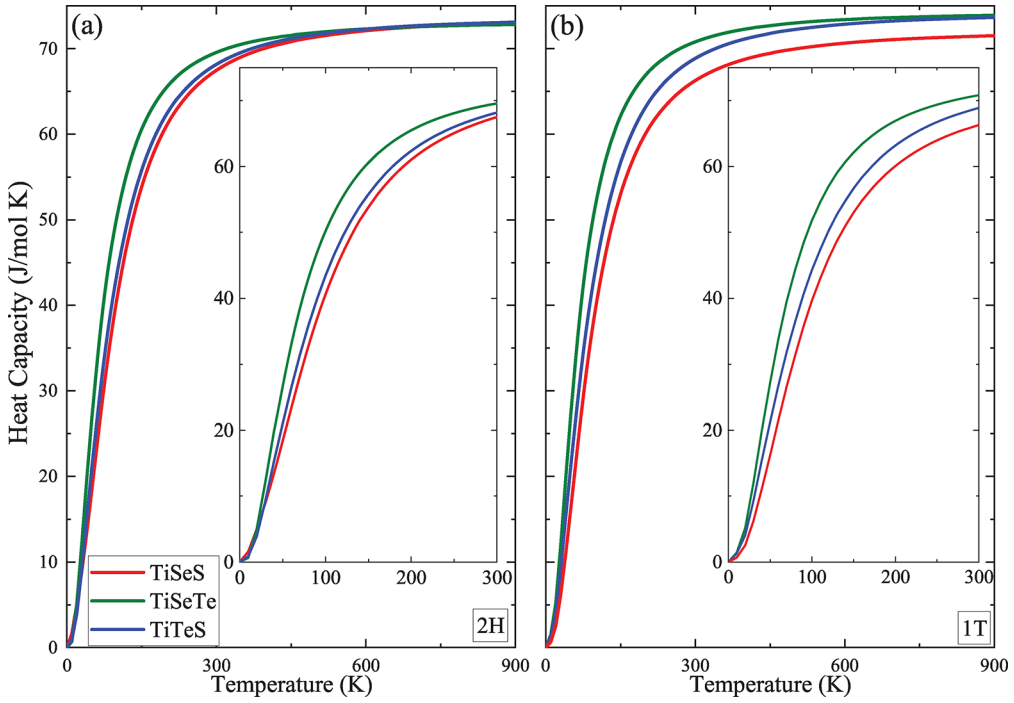

Figure 6. Variation of heat capacity (C_v) of (a) 2H- and (b) 1T-TiXY with temperature. Low-temperature behavior (up to room temperature) of C_v is given as an inset.

system but also how quickly it radiates heat. Heat capacity at constant volume can be calculated by[51]

$$C_v = \sum_{qs} k_B \left(\frac{\hbar\omega_s(q)}{k_B T}\right)^2 \frac{\exp(\hbar\omega_s(q)/k_B T)}{[\exp(\hbar\omega_s(q)/k_B T - 1]^2} \quad (3)$$

where q is the wave vector; $\omega_s(q)$ is the phonon frequency at q with phonon mode index s; T is the temperature; k_B is the Boltzmann constant; and $\hbar$ is the reduced Planck constant. As expected, C_v increases with temperature for all compositions and converges to a constant value of 3NR (3×24 J·K^{-1}·mol^{-1}), approaching the Dulong−Petit limit as shown in Figure 6a,b. It is noticed that 1T-TiSeS deviates from this limit due to imaginary phonon frequencies, but the C_v of 1T-TiSeS is also included for the sake of completeness. Up to 300 K, C_v slightly increases down the chalcogen group for both phases. It can be correlated with the shift of optical modes, as C_v varies much faster for high-frequency optical phonon modes than low-frequency acoustic phonon modes at low-temperature values.[65]

Charge Density Wave Instability in 1T-TiSeS. As shown in Figure 2b, the ZA phonon branch of 1T-TiSeS becomes imaginary around the M point which indicates a CDW transition similar to that observed in 1T-$TiSe_2$.[25,57] For the symmetric system, the band structure near E_F consists of a pair of concave bands which are mainly derived from the Se−S 4p states. At the M point, the bottom of a convex band reaches just below E_F, and this band is derived from the Ti 3d states, yielding a negative gap of 371 meV. For the 2×2 distorted phase (Figure 7a), the semimetallic state is altered, and the gap opening is noticed as shown in Figure 7c due to Peierls distortion.[66] E_{gap} is obtained as 0.08 (0.07) eV with GGA-PBE (+SOC) and 0.36 eV with HSE06 (Figure S3, Supporting Information). The calculated atomic displacements in the CDW phase are 0.09 Å for Ti and 0.03 Å for Se and S atoms. While d_{Ti-S} (d_{Ti-Se}) is equal to 2.41 Å (2.58 Å) for symmetric configurations, it becomes 2.36 Å, 2.41 Å, and 2.47 Å (2.51 Å, 2.58 Å, and 2.65 Å) in the distorted phase (Figure 7a). The total energy per chemical unit is lowered by 3 meV for the distorted (CDW) phase relative to the symmetric one, and no imaginary phonon modes are noticed (Figure 7b). Gap opening pushes the occupied Se−S 4p states to lower energies, resulting in total energy lowering. For ternary systems, this is counteracted by an increase in elastic energy so that CDW transition is not observed in 1T-TiSeTe and 1T-TiTeS. The CDW phase is entirely a band structure effect as a result of spontaneous symmetry breaking involving atomic displacements similar to $TiSe_2$.

CONCLUSIONS

In summary, we investigated the structural, mechanical, electronic, thermal, and optical properties of TiXY (X/Y = S, Se, and Te) monolayers. In addition to the mostly studied 1T phase, the 2H phase was also considered, and the stability of both phases was demonstrated by phonon spectrum analysis and high-temperature molecular dynamics simulations. The electronic structure analysis indicated that while 1T-TiXY monolayers are semimetallic with negative band gap all 2H-TiXY are indirect band gap semiconductors. Accordingly, the semiconducting phases have absorption in the visible and infrared regions, and the Drude peak is obtained for semimetallic 1T-TiXY in the low-frequency regime. Finally, the variation of heat capacity with temperature showed that C_v slightly increases down in the chalcogen group which can be correlated with the shift of optical modes and then converges to the Dulong−Petit limit at higher temperatures. Finally, together with symmetric configurations, distorted phases were also taken into account, and charge density wave transition in 1T-TiSeS due to Peierls instability was revealed. The energy lowering due to band gap opening is counteracted by an increase in elastic energy, so that CDW transition is not observed in other metallic systems. Our results not only reveal the stable Janus structures of 2H- and 1T-

DOI: 10.1021/acs.jpcc.9b06925
J. Phys. Chem. C 2019, 123, 29922−29931

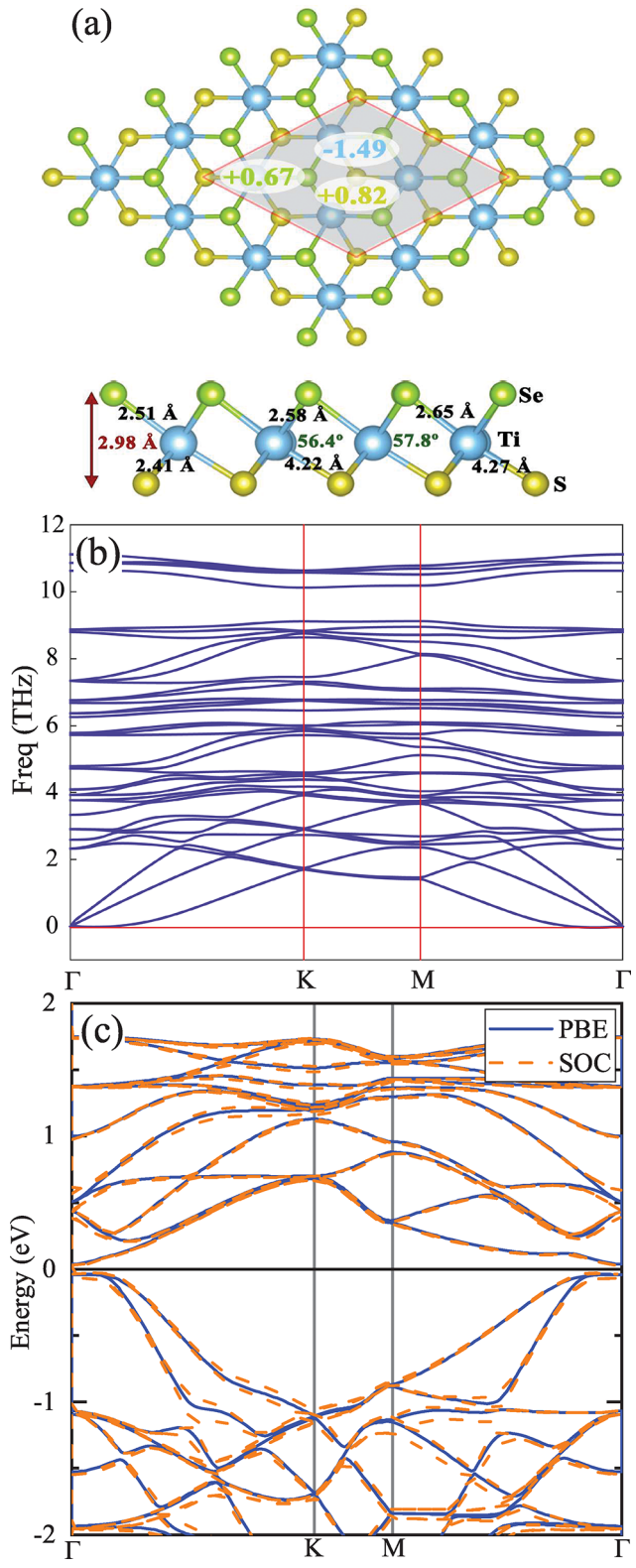

Figure 7. (a) Structure, (b) phonon dispersion, and (c) electronic band structure of the distorted 1T-TiSeS monolayer for the 2 × 2 super cell.

TiXY monolayers but also characterization of their fundamental properties suggests these systems as promising candidates for nanoscale applications.

■ ASSOCIATED CONTENT

Supporting Information

The Supporting Information is available free of charge at https://pubs.acs.org/doi/10.1021/acs.jpcc.9b06925.

The electronic band structures of 1T- and 2H-TiXY monolayers, the frequency-dependent imaginary dielectric function of 2H-TiXY monolayers, and the electronic band structure of distorted 1T-TiSeS calculated at the level of HSE06 (PDF)

■ AUTHOR INFORMATION

Corresponding Author

*E-mail: durgun@unam.bilkent.edu.tr.

ORCID

E. Durgun: 0000-0002-0639-5862

Notes

The authors declare no competing financial interest.

■ ACKNOWLEDGMENTS

The calculations were performed at TUBITAK ULAKBIM, High Performance and Grid Computing Center (TR-Grid e-Infrastructure), and the National Center for High Performance Computing of Turkey (UHeM) under Grant No. 5003622015. This work was supported by the Scientific and Technological Research Council of Turkey (TUBITAK) under Project No. 117F383. Authors acknowledge the Ankara University for a high performance computing facility through the AYP under Grant No. 17A0443001. S.J. acknowledges support from The Turkish Academy of Sciences Outstanding Young Scientists Award Program (TUBA-GEBIP).

■ REFERENCES

(1) Rasmussen, F. A.; Thygesen, K. S. Computational 2D materials database: electronic structure of transition-metal dichalcogenides and oxides. *J. Phys. Chem. C* **2015**, *119*, 13169−13183.

(2) Ataca, C.; Sahin, H.; Ciraci, S. Stable, single-layer MX_2 transition-metal oxides and dichalcogenides in a honeycomb-like structure. *J. Phys. Chem. C* **2012**, *116*, 8983−8999.

(3) Manzeli, S.; Ovchinnikov, D.; Pasquier, D.; Yazyev, O. V.; Kis, A. 2D transition metal dichalcogenides. *Nat. Rev. Mater.* **2017**, *2*, 17033.

(4) Wang, Q. H.; Kalantar-Zadeh, K.; Kis, A.; Coleman, J. N.; Strano, M. S. Electronics and optoelectronics of two-dimensional transition metal dichalcogenides. *Nat. Nanotechnol.* **2012**, *7*, 699.

(5) Mak, K. F.; Shan, J. Photonics and optoelectronics of 2D semiconductor transition metal dichalcogenides. *Nat. Photonics* **2016**, *10*, 216.

(6) Chhowalla, M.; Shin, H. S.; Eda, G.; Li, L.-J.; Loh, K. P.; Zhang, H. The chemistry of two-dimensional layered transition metal dichalcogenide nanosheets. *Nat. Chem.* **2013**, *5*, 263.

(7) Radisavljevic, B.; Radenovic, A.; Brivio, J.; Giacometti, i. V.; Kis, A. Single-layer MoS_2 transistors. *Nat. Nanotechnol.* **2011**, *6*, 147.

(8) Ross, J. S.; Klement, P.; Jones, A. M.; Ghimire, N. J.; Yan, J.; Mandrus, D.; Taniguchi, T.; Watanabe, K.; Kitamura, K.; Yao, W.; et al. Electrically tunable excitonic light-emitting diodes based on monolayer WSe_2 p−n junctions. *Nat. Nanotechnol.* **2014**, *9*, 268.

(9) Lopez-Sanchez, O.; Lembke, D.; Kayci, M.; Radenovic, A.; Kis, A. Ultrasensitive photodetectors based on monolayer MoS_2. *Nat. Nanotechnol.* **2013**, *8*, 497.

(10) Baugher, B. W.; Churchill, H. O.; Yang, Y.; Jarillo-Herrero, P. Optoelectronic devices based on electrically tunable p−n diodes in a monolayer dichalcogenide. *Nat. Nanotechnol.* **2014**, *9*, 262.

(11) Chen, X.; McDonald, A. R. Functionalization of two-dimensional transition-metal dichalcogenides. *Adv. Mater.* **2016**, *28*, 5738−5746.

DOI: 10.1021/acs.jpcc.9b06925
J. Phys. Chem. C 2019, 123, 29922−29931

(12) Voiry, D.; Goswami, A.; Kappera, R.; e Silva, C. d. C. C.; Kaplan, D.; Fujita, T.; Chen, M.; Asefa, T.; Chhowalla, M. Covalent functionalization of monolayered transition metal dichalcogenides by phase engineering. *Nat. Chem.* **2015**, *7*, 45.
(13) Conley, H. J.; Wang, B.; Ziegler, J. I.; Haglund, R. F., Jr; Pantelides, S. T.; Bolotin, K. I. Bandgap engineering of strained monolayer and bilayer MoS_2. *Nano Lett.* **2013**, *13*, 3626−3630.
(14) Liu, Q.; Li, L.; Li, Y.; Gao, Z.; Chen, Z.; Lu, J. Tuning electronic structure of bilayer MoS_2 by vertical electric field: a first-principles investigation. *J. Phys. Chem. C* **2012**, *116*, 21556−21562.
(15) Geim, A. K.; Grigorieva, I. V. Van der Waals heterostructures. *Nature* **2013**, *499*, 419.
(16) Lin, C.; Zhu, X.; Feng, J.; Wu, C.; Hu, S.; Peng, J.; Guo, Y.; Peng, L.; Zhao, J.; Huang, J.; et al. Hydrogen-incorporated TiS_2 ultrathin nanosheets with ultrahigh conductivity for stamp-transferrable electrodes. *J. Am. Chem. Soc.* **2013**, *135*, 5144−5151.
(17) Zeng, Z.; Yin, Z.; Huang, X.; Li, H.; He, Q.; Lu, G.; Boey, F.; Zhang, H. Single-Layer Semiconducting Nanosheets: High-yield preparation and device fabrication. *Angew. Chem., Int. Ed.* **2011**, *50*, 11093−11097.
(18) Wang, J.; Zheng, H.; Xu, G.; Sun, L.; Hu, D.; Lu, Z.; Liu, L.; Zheng, J.; Tao, C.; Jiao, L. Controlled synthesis of two-dimensional 1T-$TiSe_2$ with charge density wave transition by chemical vapor transport. *J. Am. Chem. Soc.* **2016**, *138*, 16216−16219.
(19) Peng, J.-P.; Guan, J.-Q.; Zhang, H.-M.; Song, C.-L.; Wang, L.; He, K.; Xue, Q.-K.; Ma, X.-C. Molecular beam epitaxy growth and scanning tunneling microscopy study of $TiSe_2$ ultrathin films. *Phys. Rev. B: Condens. Matter Mater. Phys.* **2015**, *91*, 121113.
(20) Chen, P.; Pai, W. W.; Chan, Y.-H.; Takayama, A.; Xu, C.-Z.; Karn, A.; Hasegawa, S.; Chou, M.-Y.; Mo, S.-K.; Fedorov, A.-V.; et al. Emergence of charge density waves and a pseudogap in single-layer $TiTe_2$. *Nat. Commun.* **2017**, *8*, 516.
(21) Yan, C.; Gong, C.; Wangyang, P.; Chu, J.; Hu, K.; Li, C.; Wang, X.; Du, X.; Zhai, T.; Li, Y.; et al. 2D group IVB transition metal dichalcogenides. *Adv. Funct. Mater.* **2018**, *28*, 1803305.
(22) Varma, S. J.; Kumar, J.; Liu, Y.; Layne, K.; Wu, J.; Liang, C.; Nakanishi, Y.; Aliyan, A.; Yang, W.; Ajayan, P. M.; et al. 2D TiS_2 layers: a superior nonlinear optical limiting material. *Adv. Opt. Mater.* **2017**, *5*, 1700713.
(23) Wan, C.; Tian, R.; Kondou, M.; Yang, R.; Zong, P.; Koumoto, K. Ultrahigh thermoelectric power factor in flexible hybrid inorganic-organic superlattice. *Nat. Commun.* **2017**, *8*, 1024.
(24) Sherrell, P. C.; Sharda, K.; Grotta, C.; Ranalli, J.; Sokolikova, M. S.; Pesci, F. M.; Palczynski, P.; Bemmer, V. L.; Mattevi, C. Thickness-Dependent Characterization of Chemically Exfoliated TiS_2 Nanosheets. *ACS Omega* **2018**, *3*, 8655−8662.
(25) Chen, P.; Chan, Y.-H.; Fang, X.-Y.; Zhang, Y.; Chou, M.-Y.; Mo, S.-K.; Hussain, Z.; Fedorov, A.-V.; Chiang, T.-C. Charge density wave transition in single-layer titanium diselenide. *Nat. Commun.* **2015**, *6*, 8943.
(26) Ganesh, R.; Baskaran, G.; van den Brink, J.; Efremov, D. V. Theoretical prediction of a time-reversal broken chiral superconducting phase driven by electronic correlations in a single TiSe2 layer. *Phys. Rev. Lett.* **2014**, *113*, 177001.
(27) Lu, A.-Y.; Zhu, H.; Xiao, J.; Chuu, C.-P.; Han, Y.; Chiu, M.-H.; Cheng, C.-C.; Yang, C.-W.; Wei, K.-H.; Yang, Y.; et al. Janus monolayers of transition metal dichalcogenides. *Nat. Nanotechnol.* **2017**, *12*, 744.
(28) Zhang, J.; Jia, S.; Kholmanov, I.; Dong, L.; Er, D.; Chen, W.; Guo, H.; Jin, Z.; Shenoy, V. B.; Shi, L.; et al. Janus monolayer transition-metal dichalcogenides. *ACS Nano* **2017**, *11*, 8192−8198.
(29) Gao, T.; Zhang, Q.; Li, L.; Zhou, X.; Li, L.; Li, H.; Zhai, T. 2D ternary chalcogenides. *Adv. Opt. Mater.* **2018**, *6*, 1800058.
(30) Wang, L.; Hu, P.; Long, Y.; Liu, Z.; He, X. Recent advances in ternary two-dimensional materials: synthesis, properties and applications. *J. Mater. Chem. A* **2017**, *5*, 22855−22876.
(31) Li, L.; Gong, P.; Wang, W.; Deng, B.; Pi, L.; Yu, J.; Zhou, X.; Shi, X.; Li, H.; Zhai, T. Strong in-plane anisotropies of optical and electrical response in layered dimetal chalcogenide. *ACS Nano* **2017**, *11*, 10264−10272.
(32) Jia, Q.; Zhang, Y. C.; Li, J.; Chen, Y.; Xu, B. Hydrothermal synthesis of Cu_2WS_4 as a visible-light-activated photocatalyst in the reduction of aqueous Cr (VI). *Mater. Lett.* **2014**, *117*, 24−27.
(33) Wu, J.; Yuan, H.; Meng, M.; Chen, C.; Sun, Y.; Chen, Z.; Dang, W.; Tan, C.; Liu, Y.; Yin, J.; et al. High electron mobility and quantum oscillations in non-encapsulated ultrathin semiconducting Bi_2O_2Se. *Nat. Nanotechnol.* **2017**, *12*, 530.
(34) Lee, J.-U.; Lee, S.; Ryoo, J. H.; Kang, S.; Kim, T. Y.; Kim, P.; Park, C.-H.; Park, J.-G.; Cheong, H. Ising-type magnetic ordering in atomically thin $FePS_3$. *Nano Lett.* **2016**, *16*, 7433−7438.
(35) Cabán-Acevedo, M.; Stone, M. L.; Schmidt, J.; Thomas, J. G.; Ding, Q.; Chang, H.-C.; Tsai, M.-L.; He, J.-H.; Jin, S. Efficient hydrogen evolution catalysis using ternary pyrite-type cobalt phosphosulphide. *Nat. Mater.* **2015**, *14*, 1245.
(36) Gong, C.; Li, L.; Li, Z.; Ji, H.; Stern, A.; Xia, Y.; Cao, T.; Bao, W.; Wang, C.; Wang, Y.; et al. Discovery of intrinsic ferromagnetism in two-dimensional van der Waals crystals. *Nature* **2017**, *546*, 265.
(37) Shi, W.; Wang, Z. Mechanical and electronic properties of Janus monolayer transition metal dichalcogenides. *J. Phys.: Condens. Matter* **2018**, *30*, 215301.
(38) Dong, L.; Lou, J.; Shenoy, V. B. Large in-plane and vertical piezoelectricity in Janus transition metal dichalchogenides. *ACS Nano* **2017**, *11*, 8242−8248.
(39) Li, F.; Wei, W.; Zhao, P.; Huang, B.; Dai, Y. Electronic and optical properties of pristine and vertical and lateral heterostructures of Janus MoSSe and WSSe. *J. Phys. Chem. Lett.* **2017**, *8*, 5959−5965.
(40) Kohn, W.; Sham, L. J. Self-consistent equations including exchange and correlation effects. *Phys. Rev.* **1965**, *140*, A1133.
(41) Hohenberg, P.; Kohn, W. Inhomogeneous electron gas. *Phys. Rev.* **1964**, *136*, B864.
(42) Kresse, G.; Furthmüller, J. Efficient iterative schemes for ab initio total-energy calculations using a plane-wave basis set. *Phys. Rev. B: Condens. Matter Mater. Phys.* **1996**, *54*, 11169.
(43) Perdew, J. P.; Burke, K.; Ernzerhof, M. Generalized gradient approximation made simple. *Phys. Rev. Lett.* **1996**, *77*, 3865.
(44) Blöchl, P. E. Projector augmented-wave method. *Phys. Rev. B: Condens. Matter Mater. Phys.* **1994**, *50*, 17953.
(45) Kresse, G.; Joubert, D. From ultrasoft pseudopotentials to the projector augmented-wave method. *Phys. Rev. B: Condens. Matter Mater. Phys.* **1999**, *59*, 1758.
(46) Monkhorst, H. J.; Pack, J. D. Special points for Brillouin-zone integrations. *Phys. Rev. B* **1976**, *13*, 5188.
(47) Heyd, J.; Scuseria, G. E.; Ernzerhof, M. Hybrid functionals based on a screened Coulomb potential. *J. Chem. Phys.* **2003**, *118*, 8207−8215.
(48) Krukau, A. V.; Vydrov, O. A.; Izmaylov, A. F.; Scuseria, G. E. Influence of the exchange screening parameter on the performance of screened hybrid functionals. *J. Chem. Phys.* **2006**, *125*, 224106.
(49) Tang, W.; Sanville, E.; Henkelman, G. A grid-based Bader analysis algorithm without lattice bias. *J. Phys.: Condens. Matter* **2009**, *21*, 084204.
(50) Yu, M.; Trinkle, D. R. Accurate and efficient algorithm for Bader charge integration. *J. Chem. Phys.* **2011**, *134*, 064111.
(51) Togo, A.; Tanaka, I. First principles phonon calculations in materials science. *Scr. Mater.* **2015**, *108*, 1−5.
(52) Pines, D.; Bohm, D. A collective description of electron interactions: II. Collective vs individual particle aspects of the interactions. *Phys. Rev.* **1952**, *85*, 338.
(53) Singh, B.; Hsu, C.-H.; Tsai, W.-F.; Pereira, V. M.; Lin, H. Stable charge density wave phase in a 1 T−$TiSe_2$ monolayer. *Phys. Rev. B: Condens. Matter Mater. Phys.* **2017**, *95*, 245136.
(54) Li, G.; Yao, K.; Gao, G. Strain-induced enhancement of thermoelectric performance of TiS_2 monolayer based on first-principles phonon and electron band structures. *Nanotechnology* **2018**, *29*, 015204.
(55) Zhang, X.; Qiao, X.-F.; Shi, W.; Wu, J.-B.; Jiang, D.-S.; Tan, P.-H. Phonon and Raman scattering of two-dimensional transition metal

DOI: 10.1021/acs.jpcc.9b06925
J. Phys. Chem. C 2019, 123, 29922−29931

dichalcogenides from monolayer, multilayer to bulk material. *Chem. Soc. Rev.* **2015**, *44*, 2757−2785.
(56) Kohn, W. Image of the Fermi Surface in the Vibration Spectrum of a Metal. *Phys. Rev. Lett.* **1959**, *2*, 393.
(57) Guster, B.; Canadell, E.; Pruneda, M.; Ordejón, P. First principles analysis of the CDW instability of single-layer 1T-$TiSe_2$ and its evolution with charge carrier density. *2D Mater.* **2018**, *5*, 025024.
(58) Fu, Z.-G.; Wang, J.-H.; Yang, Y.; Yang, W.; Liu, L.-L.; Hu, Z.-Y.; Zhang, P. Doping stability and charge-density-wave transition of strained 1T-$TiSe_2$. *EPL (Europhysics Letters)* **2017**, *120*, 17006.
(59) Wei, M.; Lu, W.; Xiao, R.; Lv, H.; Tong, P.; Song, W.; Sun, Y. Manipulating charge density wave order in monolayer 1 T- $TiSe_2$ by strain and charge doping: A first-principles investigation. *Phys. Rev. B: Condens. Matter Mater. Phys.* **2017**, *96*, 165404.
(60) Xiao, R.; Lu, W.; Shao, D.; Li, J.; Wei, M.; Lv, H.; Tong, P.; Zhu, X.; Sun, Y. Manipulating superconductivity of 1 T-$TiTe_2$ by high pressure. *J. Mater. Chem. C* **2017**, *5*, 4167−4173.
(61) Born, M. On the stability of crystal lattices. I. *Math. Proc. Cambridge Philos. Soc.* **1940**, *36*, 160−172.
(62) Frantsevich, N.; Voronov, F.; Bakuta, S. *Handbook on Elastic Constants and Moduli of Elasticity for Metals and Nonmetals*; Naukova Dumka: Kiev, 1982.
(63) Lanzillo, N. A.; Simbeck, A. J.; Nayak, S. K. Strain engineering the work function in monolayer metal dichalcogenides. *J. Phys.: Condens. Matter* **2015**, *27*, 175501.
(64) Song, S. M.; Park, J. K.; Sul, O. J.; Cho, B. J. Determination of work function of graphene under a metal electrode and its role in contact resistance. *Nano Lett.* **2012**, *12*, 3887−3892.
(65) Qin, G.; Qin, Z.; Wang, H.; Hu, M. Anomalously temperature-dependent thermal conductivity of monolayer GaN with large deviations from the traditional 1/T law. *Phys. Rev. B: Condens. Matter Mater. Phys.* **2017**, *95*, 195416.
(66) Kidd, T.; Miller, T.; Chou, M.; Chiang, T.-C. Electron-hole coupling and the charge density wave transition in $TiSe_2$. *Phys. Rev. Lett.* **2002**, *88*, 226402.

DOI: 10.1021/acs.jpcc.9b06925
J. Phys. Chem. C 2019, 123, 29922−29931